Separation and Purification Technology 329 (2024) 125167

Contents lists available at ScienceDirect

Separation and Purification Technology

journal homepage: www.elsevier.com/locate/seppur

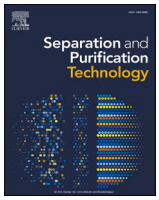

A thermostable calcium-based metal–organic framework for efficient capture and separation of acetylene from ternary mixture

Shan-Qing Yang [a], Rajamani Krishna [b], Lei Zhou [a], Yi-Long Li [a], Bo Xing [a], Qiang Zhang [a], Fei-Yang Zhang [a], Tong-Liang Hu [a,*]

[a] School of Materials Science and Engineering, National Institute for Advanced Materials, Nankai University, Tianjin 300350, China
[b] Van 't Hoff Institute for Molecular Sciences, University of Amsterdam, Science Park 904, 1098 XH Amsterdam, the Netherlands

ARTICLE INFO

Keywords:
Ca-based metal–organic framework
Gas capture and separation
C_2H_2 purification
Multiple component mixture separation

ABSTRACT

High-efficiency and eco-friendly selective separation of C_2H_2 from industrial gaseous mixtures such as CO_2 and CH_4 is of great importance in the purification and production of downstream commodity chemicals. Herein, we report a thermostable calcium-based metal–organic framework, namely **NUM-20**, which could preferentially capture C_2H_2 from C_2H_2-containing gaseous mixtures. **NUM-20** exhibits a higher capacity and preferential adsorption behavior of C_2H_2 versus the competing gases including CO_2 and CH_4, as reflected by single component gas sorption isotherms and the heat of adsorption. The IAST selectivity calculations indicate that **NUM-20** possesses multiple component separation capacity, and the transient breakthrough simulations were performed to validate the capture and separation of C_2H_2 from multiple components. Furthermore, computational simulations were carried out to unveil the host–guest interactions under the molecular-level. This study on Ca-based MOF materials will enrich the three-dimensional Ca-based MOF adsorbents for gas capture and separation applications and address the industrial challenging separation process.

1. Introduction

The separation and purification of light hydrocarbons with an energy-efficient and environmentally manner is of great significance to the petrochemical industrial [1]. Generally, light hydrocarbons such as acetylene (C_2H_2) are widely used to produce many high value-added chemicals including rubber, fibers, plastics, vinyl compounds, acrylic acid etc. [2]. As the simplest alkyne, acetylene is one of the most significant raw materials in the electronic and petrochemical industries, and the industrial production of C_2H_2 is usually depended on energy-intensive state-of-the-art, including the steam cracking of naphtha and/or methane (CH_4) combustion, resulting the energy footprint and producing waste, and these processes often co-produce other gases such as carbon dioxide (CO_2) and CH_4 [3–5], which tremendously degrade the significance of C_2H_2. Therefore, the capture and separation of C_2H_2 from C_2H_2-containing mixtures including CO_2 and CH_4 is a very significant industrial process to obtain the pure C_2H_2 substance. However, their similar physical properties, such as molecular size (C_2H_2: 3.32 × 3.34 × 5.70 Å^3, CO_2: 3.18 × 3.33 × 5.36 Å^3, CH_4: 3.70 × 3.70 × 3.70 Å^3, respectively), kinetic diameter (C_2H_2: 3.3 Å, CO_2: 3.3 Å, CH_4: 3.8 Å, respectively), and boiling point (C_2H_2: 189.3 K, CO_2: 194.7 K, CH_4: 111.6 K, respectively) (Scheme 1) [6–8], make the separation task become a daunting challenge. Diverse porous solid adsorbents have been used to separate light hydrocarbons via pressure or temperature swing adsorption, i.e., the PSA or TSA processes. Compared with the traditional cryogenic distillation or chemical absorption, these processes are more green, environmentally friendly, and efficient. Under this context, it is not at all surprising to realize the recent increasingly in research interest to develop porous solid adsorbents for selective C_2H_2 capture from the mixtures of industrial relevance, such as C_2H_2/CO_2 and C_2H_2/CH_4 [9–17].

The core of the adsorptive separation process is the adsorbent material, which impacts the adsorption and separation performance. As a significant class of crystal porous solid materials, metal–organic frameworks (MOFs) or coordination polymers (CPs) featuring structural tunability and diverse functionality, self-assembled by metal ions/clusters nodes and organic ligands linkers through non-covalent-coordinate bonds [18–21], have obtained more attention as promising candidate porous adsorbents for gas capture and separation. Among the various of porous solid MOFs reported so far, those comprising biocompatible

* Corresponding author.
E-mail address: tlhu@nankai.edu.cn (T.-L. Hu).

https://doi.org/10.1016/j.seppur.2023.125167
Received 22 July 2023; Received in revised form 19 September 2023; Accepted 19 September 2023
Available online 21 September 2023

metals such as calcium-based MOFs (Ca-MOFs) are of particular interest. Compared to lanthanide-metal-based or transitional metals-based MOF analogues, the Ca-MOFs enjoy exceptional advantages such as high thermal stability, low toxicity and earth-abundant of Ca^{2+} [22]. However, the three-dimensional Ca-MOFs are underexplored, which may be attributed to inherent challenges including the high coordination number of Ca^{2+} and unpredictable coordination geometry etc. In this regard, constructing new Ca-MOFs is in favor of exploring potential application on gas capture and separation field. Currently, the unique characteristics of MOF materials make it realize the enormous accomplishments with respect to the design and construction of target adsorbents with ideal properties for challenging gas separations. For example, a number of MOF materials that could selectively trap C_2H_2 from CO_2 and light hydrocarbons, especially C_1-C_2 hydrocarbons have been reported [2,23–32], but the reported capture of C_2H_2 from $C_2H_2/CH_4/CO_2$ ternary mixtures to simulate the intricate industrial gas mixtures is yet still rare [33,34]. In particular, the systematic study of Ca-MOFs as adsorbents for the capture and separation of C_2H_2 from such ternary mixture is uncommon. Under this context, developing and constructing novel Ca-MOFs for the capture and separation of C_2H_2 from multicomponent mixtures is one-stone-two-birds strategy, which not only enriches new Ca-based MOF materials but also addresses challenging multicomponent mixtures separation with efficient multifunctional adsorbents.

With this in mind, we successfully synthesized a new thermostable Ca-based metal–organic framework (**NUM-20**) that could selectively capture C_2H_2 from multicomponent mixtures including C_2H_2, CO_2, and CH_4. And the systematic research on C_2H_2-selective adsorption behavior of the prepared **NUM-20** was carried out by experimental and computational methods. Single component gas adsorption exhibited the **NUM-20** has a decent C_2H_2 capacity under the ambient conditions, with low adsorption capacity for CO_2 and CH_4. This led to well ideal adsorption solution theory (IAST) selectivities of 174.5/99.3 for C_2H_2/CH_4 and 5.3/5.4 for C_2H_2/CO_2 at 273/298 K and 1.0 bar, comparable to the same type of MOFs reported by far. The results of adsorption enthalpy revealed that the strongest binding affinity toward C_2H_2 among those for CO_2 and CH_4. Moreover, transient breakthrough simulations demonstrated the selective capture and separation of C_2H_2 on **NUM-20** from multicomponent mixtures. In addition, grand canonical Monte Carlo (GCMC) simulations afforded a molecular level insight to in-depth understand the host–guest interactions. Combined the experimental and computational results, **NUM-20** could efficiently trap C_2H_2 from binary mixtures (C_2H_2/CH_4 and C_2H_2/CO_2), and $C_2H_2/CO_2/CH_4$ ternary mixture to realize enrich C_2H_2 stream target. This study on capture and separation of acetylene from multicomponent mixtures with thermostable Ca-MOF will enrich Ca-MOF materials for gas adsorption and separation applications.

2. Experimental

2.1. Materials and methods

All the reagents and solvents were purchased from commercial suppliers and used without further purification. Powder X-ray diffraction (PXRD) patterns were collected on a Rigaku MiniFlex 600 at 40 kV and 15 mA with a scan rate of 8.0° min^{-1} using Cu Kα (λ = 1.5418 Å) radiation in an air atmosphere. Thermogravimetric analysis (TGA) study was performed on a Rigaku standard thermogravimetry–differential thermal analysis (TG-DTA) analyzer from room temperature to 800 °C under air atmosphere with a heating rate of 10 °C min^{-1}, using an empty and clean Al_2O_3 crucible as a reference.

2.2. Synthesis of NUM-20

$Ca(NO_3)_2{\cdot}4H_2O$ (50.0 mg, 0.2 mmol) and 1,3,6,8-Tetra(4-carboxylphenyl) pyrene ligand (H_4TBAPy, 5.0 mg, 0.007 mmol) were dissolved in N,N-dimethyl formamide (DMF, 2 mL), deionized water (0.3 mL) and nitric acid (2 M, 2 drops) in a 10 mL glass vial. The vial was tightly capped and placed in an oven preheated to 365 K. After the vial remained undisturbed at this temperature for 48 h, the white rhombic crystals formed were obtained by suction filtration and washed with fresh DMF several times. Yield: 75% based on H_4TBAPy.

2.3. Activation of NUM-20

The fresh sample **NUM-20** was guest exchanged with chromatographic pure acetone for 6 h and the solvent-exchange sample was evacuated under vacuum conditions (less than 10^{-5} Torr) at 423 K for 8 h to obtain the activated **NUM-20**.

2.4. Single crystal X-ray diffraction (SCXRD)

Crystallographic data of **NUM-20** were recorded on a Rigaku XtaLAB Pro MM007HF DW diffractometer equipped with the graphite-monochromatic Cu-Kα radiation (λ = 1.54184 Å). The structure was solved using direct methods and refined with full-matrix least-squares refinement using the SHELXTL-97 crystallographic software package [35,36]. All non-hydrogen atoms were refined through anisotropic displacement parameters, and the hydrogen atoms were added to their geometrically ideal positions using the riding model. The X-ray crystallographic coordinate for structure reported in this article has been deposited at the Cambridge Crystallographic Data Centre (CCDC), under deposition CCDC number: 2279959. The data can be obtained free of charge from The Cambridge Crystallographic Data Centre via https://www.ccdc.cam.ac.uk/.

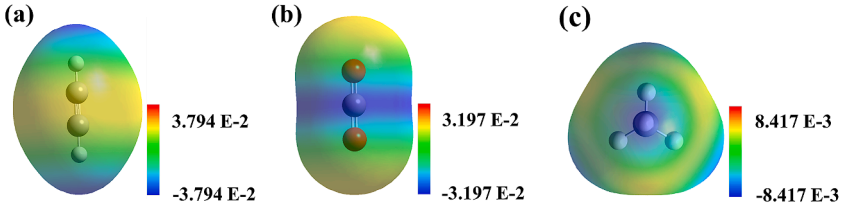

3.32 × 3.34 × 5.70	3.18 × 3.33 × 5.36	3.70 × 3.70 × 3.70	Molecular size (Å^3)
3.3	3.3	3.8	Kinetic diameter (Å)
189.3	194.7	111.6	Boiling point (K)
7.50	-4.30	0	Quadrupole moment (×10^{26}/esu cm^2)

Scheme 1. Electrostatic potentials and physiochemical properties of C_2H_2 (a), CO_2 (b), and CH_4 (c).

2.5. Gas sorption measurements

Single-component gas sorption experiments with C_2H_2, CO_2 and CH_4 were carried out on a Micromeritics ASAP 2020 analyzer applying the volumetric technique to precisely measure the amount of gas adsorbed. A sample of activated **NUM-20** (about 100 mg) was used for the sorption measurement and was maintained at 195 K with the mixture of dry ice and ethanol, and the bath temperatures of 273 and 298 K were precisely controlled with a LAUDR RP890 recirculating control system containing a mixture of ethylene glycol and water or ethyl alcohol. The cycling CO_2 adsorption measurements were performed on the Beishide BSD-PM2 gas adsorption instrument (Beishide Instrument Technology (Beijing) Co., Ltd).

2.6. GCMC simulations

The GCMC simulations were carried out for the adsorption of C_2H_2, CH_4 and CO_2 in **NUM-20** using Sorption Tools in Materials Studio package. The skeleton of **NUM-20** and gas molecules were regarded as rigid bodies. The optimal adsorption sites were simulated under 298 K and 1.0 bar by the fixed loading task and Metropolis method. The atomic partial charges of the host skeleton of **NUM-20** and all gas molecules were obtained from QEq method. The equilibration steps and the production steps were set to 5.0×10^6 and 1.0×10^7, respectively. The gas-skeleton interaction and the gas–gas interaction were characterized by the standard universal force field (UFF). The cut-off radius used for the Lennard-Jones interactions is 15.5 Å and the long-range electrostatic interactions were considered by the Ewald summation method.

3. Results and discussion

3.1. Single crystal X-ray diffraction structure and characterization

The high-quality single crystal of **NUM-20** was synthesized by solvothermal reaction of $Ca(NO_3)_2{\cdot}4H_2O$ and H_4TBAPy ligand in mixture solvents of DMF/H_2O at 365 K for 48 h. Single crystal X-ray diffraction suggested that **NUM-20** crystallizes in triclinic space group *P*-1, the asymmetric unit of **NUM-20** contains one $TBAPy^{4-}$ ligand, two crystallographically independent Ca(II) ions, and four coordinated water molecules. Both isolated Ca(II) ions coordinate with six carboxylate oxygens from four different ligands and two oxygens from two coordinated water molecules. The repeated Ca(II) ions with AABB arrangement form the infinitely extendable Ca-O chain by sharing oxygen atoms from carboxyl groups (Fig. 1a). The organic linker and metal chains self-assembled form three-dimensional framework featuring one dimensional channel (Fig. 1c, d). As calculated by PLATON, after removing the free solvent molecules, the total accessible volume of **NUM-20** is estimated to be 43.9%.

From the optical microscope image, as shown in Fig. 2a, it is distinctly seen that **NUM-20** exhibits diamond shaped block. The bulk sample phase purity of **NUM-20** was verified by powder X-ray diffraction measurements, as shown in Fig. 2b, the PXRD pattern of as-synthesized sample matched well with that of the simulated one exported from single crystal structure, indicating its high phase purity and good crystallinity. Interestingly, **NUM-20** exhibited good thermal stability. In particular, the thermal stability of **NUM-20** could reach 730 K under air atmosphere (Fig. 2c). Such good thermal stability is due to its high electropositivity, resulting in strong ionic-like bonds with carboxylates-based organic ligands [22]. In addition, the chemical stability of **NUM-20** was tested under different treatments. As shown in Figs. S1 and S2, **NUM-20** could maintain the framework in different organic solvents and even water, acid, and basic conditions. Obviously, **NUM-20** exhibits high thermal and chemical stability, which motivated us to investigate the adsorption and separation application of this material.

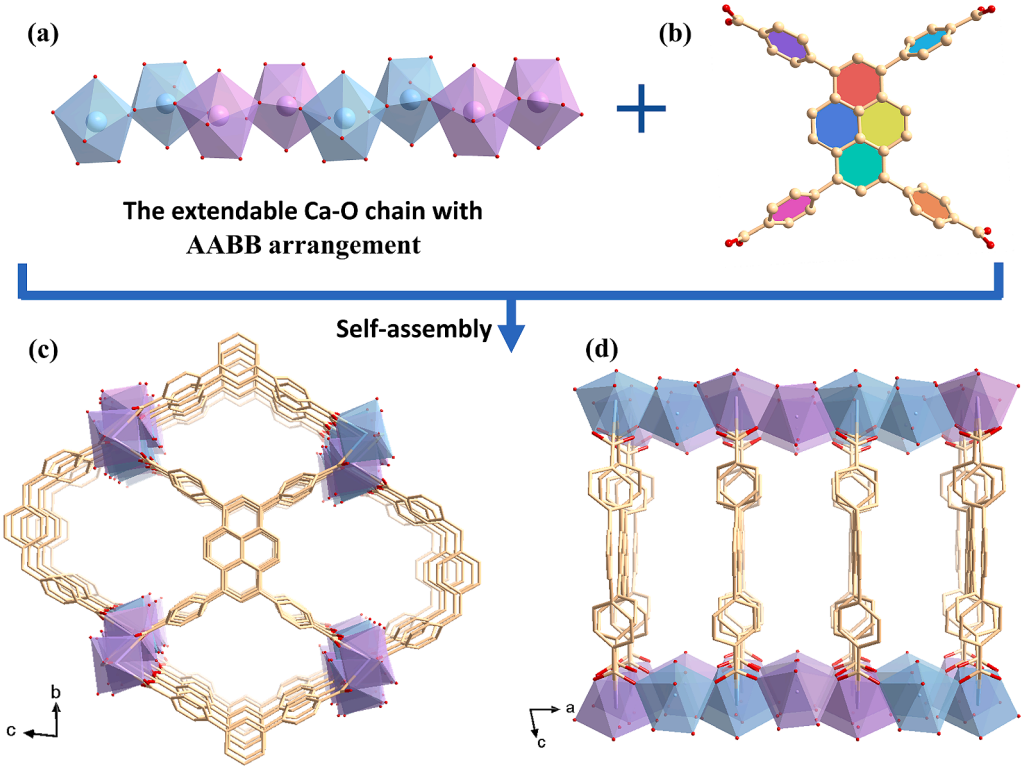

Fig. 1. Structure description of **NUM-20**. The framework of **NUM-20** formed by intensively extended Ca-O-chain with AABB arrangement (a), and $TBAPY^{4-}$ ligand (b). The one-dimensional channel in **NUM-20** as seen along the *a*-axis (c), and *b*-axis (d).

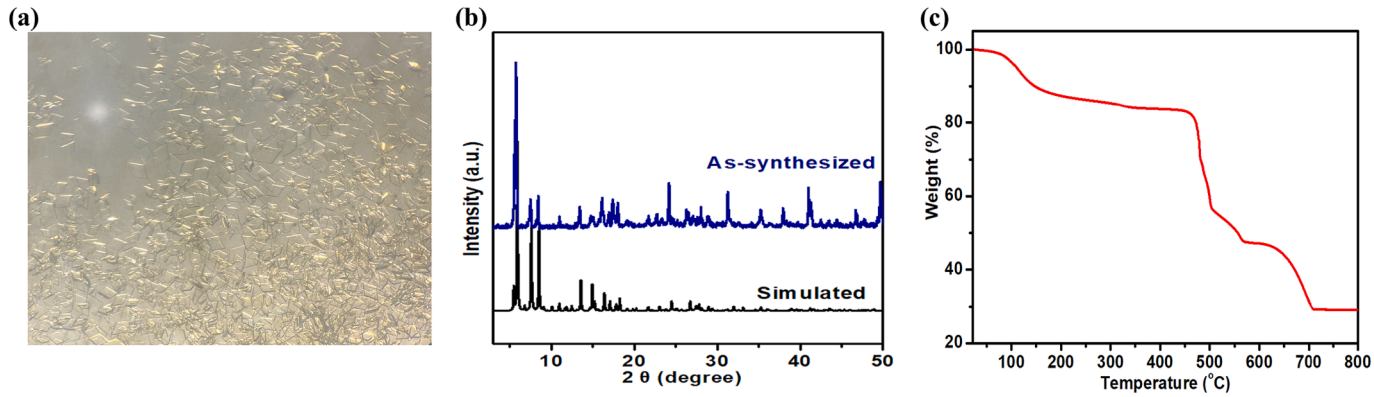

Fig. 2. (a) Optical microscope image of the crystal of **NUM-20**. (b) The experimental PXRD patterns of as-synthesized **NUM-20** sample and the simulated one from single crystal X-ray diffraction data. (c) The TG curve of **NUM-20**.

3.2. Gas sorption properties of NUM-20

The permanent porosity of activated **NUM-20** was verified by CO_2 sorption isotherms at 195 K. As shown in Fig. 3a, **NUM-20** shows a typical type I isotherm type with the CO_2 adsorption amount up to 89.65 $cm^3\ g^{-1}$ at 195 K and 1.0 bar, suggesting the microporous characteristic. The Brunauer-Emmett-Teller (BET) surface area and pore volume of **NUM-20**·were determined to be 319.17 $m^2\ g^{-1}$ and 0.189 $cm^3\ g^{-1}$, respectively. In addition, the pore-size distribution (PSD) of **NUM-20** was analyzed by employing the CO_2 sorption isotherms under 195 K according to the non-local density functional theory (NLDFT) model, which showed the microporous peaks with 8.0 Å. This pore feature is suitable for the adsorption and separation of small gas molecules.

Single-component gas adsorption isotherms of **NUM-20** for C_2H_2, CO_2 and CH_4 were examined at 273 and 298 K, respectively (Fig. 3b, c). Comparison of the C_2H_2, CO_2 and CH_4 adsorption profiles for **NUM-20** at

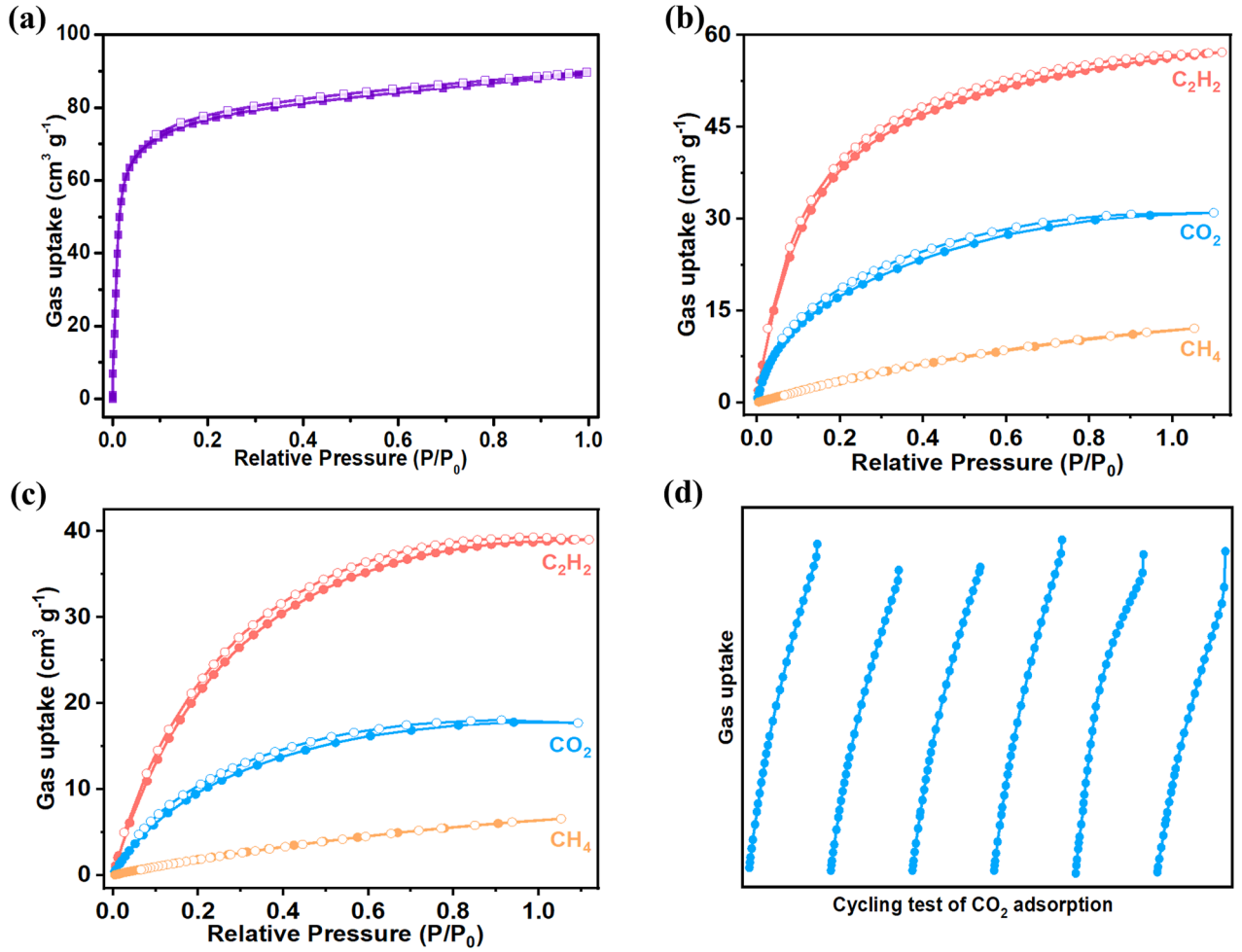

Fig. 3. (a) CO_2 adsorption and desorption isotherms of the **NUM-20** at 195 K. C_2H_2, CO_2 and CH_4 adsorption and desorption isotherms of **NUM-20** at two different temperatures of (b) 273 K, and (c) 298 K. (d) Cycling test of CO_2 adsorption measurements at 298 K. The solid and open symbols represent adsorption and desorption, respectively.

273 and 298 K indicated a strong affinity toward C_2H_2 as there were low uptakes for CO_2 and CH_4. In addition to uptake difference, the stronger binding affinity between **NUM-20** and C_2H_2 also could be reflected by the slopes of sorption isotherms in the low-pressure region. As expected, as temperature increases, the adsorption capacity of adsorbate decreases cautiously. **NUM-20** shows a distinctly preferential adsorption of C_2H_2 over CO_2 and CH_4, specifically, with a much higher C_2H_2 uptake of 57.22/39.03 $cm^3\ g^{-1}$ at 273/298 K and 1.0 bar over CO_2 (31.01/17.70 $cm^3\ g^{-1}$) and CH_4 (12.11/6.55 $cm^3\ g^{-1}$). The C_2H_2/CO_2 and C_2H_2/CH_4 uptake ratio is 185/221% and 473/596%, respectively, at 273/298 K and 1.0 bar. Notably, according to the uptake of adsorbed C_2H_2 in **NUM-20** and the corresponding pore volume, the density of adsorbed C_2H_2 in the porous adsorbent could be up to 239.7 g/L at 298 K and 1.0 bar. The packing density of C_2H_2 in **NUM-20** is about 204 times the density of gaseous C_2H_2 (1.1772 g/L, at 273 K and 101.3 kPa) and is over 114 times higher than the safe compression limit of C_2H_2 storage at 0.2 MPa (0.0021 g mL^{-1}) [37], which indicate that the C_2H_2 molecules could be efficiently packed in the porous adsorbent. Furthermore, the good density of adsorbed C_2H_2 in **NUM-20** is comparable to or higher than that of reported famous materials such as ZJU-5a (208 g/L) [38], MOF-505 (186 g/L) [39], MFM-188a (244 g/L) [40], suggesting the promising potential of C_2H_2 storage with **NUM-20**. All of those prove that **NUM-20** exhibits the preferential binding affinity with C_2H_2 over CO_2 and CH_4, and **NUM-20** could capture C_2H_2 from C_2H_2-containg mixtures. In addition, continuous CO_2 and C_2H_2 adsorption measurements on **NUM-20** were performed to prove its cycling stability. As shown in Fig. 3d and Fig. S8, **NUM-20** could maintain the uptakes of two gases after multiple cycles, suggesting its good cycling stability.

The different adsorption behavior of C_2H_2, CO_2 and CH_4 on **NUM-20** could be explained by the isosteric heat of adsorption (Q_{st}) calculated by fitting single-component adsorption isotherms in the light of virial equation model. As shown in Fig. 4a, the low coverage Q_{st} values of C_2H_2, CO_2 and CH_4 are 38.83, 37.14, and 18.86 kJ mol^{-1}, respectively, which is indeed in well line with the single component gas adsorption isotherms. The significantly higher Q_{st} for C_2H_2 over CO_2 and CH_4 indicates the strong affinity for C_2H_2 by **NUM-20**. The Q_{st} value of C_2H_2 for **NUM-20** is distinctly lower than that of other MOFs featuring open metal sites, such as Cu^I@UiO-66-$(COOH)_2$ (74.5 kJ mol^{-1}) [41], ATC-Cu (80 kJ mol^{-1}) [23], and NKMOF-1-Ni (60.3 kJ mol^{-1}) [9]. From the practical application perspective, the isosteric heat of adsorption, as an important evaluation criterion, could be representative of the regeneration energy cost in the industrial practice. The moderate adsorption enthalpy implies the probability to achieve regeneration under mild conditions (Fig. 4d), thus showing its promising potential for energy saving C_2H_2 purification from multiple components.

3.3. Gas separation properties of NUM-20

Building on the obviously difference in adsorption capacity between C_2H_2, CO_2 and CH_4 and preferential affinity indicated by the adsorption enthalpy, **NUM-20** as a new porous solid adsorbent may have the separation capacity for the binary mixtures of C_2H_2/CH_4 and C_2H_2/CO_2, and ternary mixture of $C_2H_2/CO_2/CH_4$. Thus, the adsorption selectivity of C_2H_2/CH_4 and C_2H_2/CO_2 mixtures on **NUM-20** was evaluated by ideal adsorbed solution theory (IAST) calculations to evaluate the feasibility of this separation. All selectivities values were obtained through the curve fitting the single component adsorption isotherms at 273 and 298 K. As shown in Fig. 4c, f, the IAST selectivity value of **NUM-20** is about 5.4 for equimolar C_2H_2/CO_2 binary mixture at 298 K and 1.0 bar, which is higher or comparable with the values reported for SNNU-26/27/29-Mn (1.4/1.4/2.9) [42], CAU-10*H* (4.0) [43], JNU-1 (3.6) [44], FJU-90 (4.3) [45], and UPC-200 (less than2.5) [46], MUF-17 (6.01) [47], CAU-23 (3.8) [48] etc. In addition, **NUM-20** also exhibits the well equimolar C_2H_2/CH_4 selectivity values with 174.50/99.30 at 273/298 K and 1.0 bar (Fig. 4b), which surpasses or is comparable with some reported MOFs, such as NKM-101a (28.7) [49], SBMOF-1 (33) and SBMOF-2 (18) [32], Ca-MOF (10.9) [50], BUT-318a (105.8) [51] (Fig. 4e). It is worth noting that **NUM-20** exhibits a good adsorption and

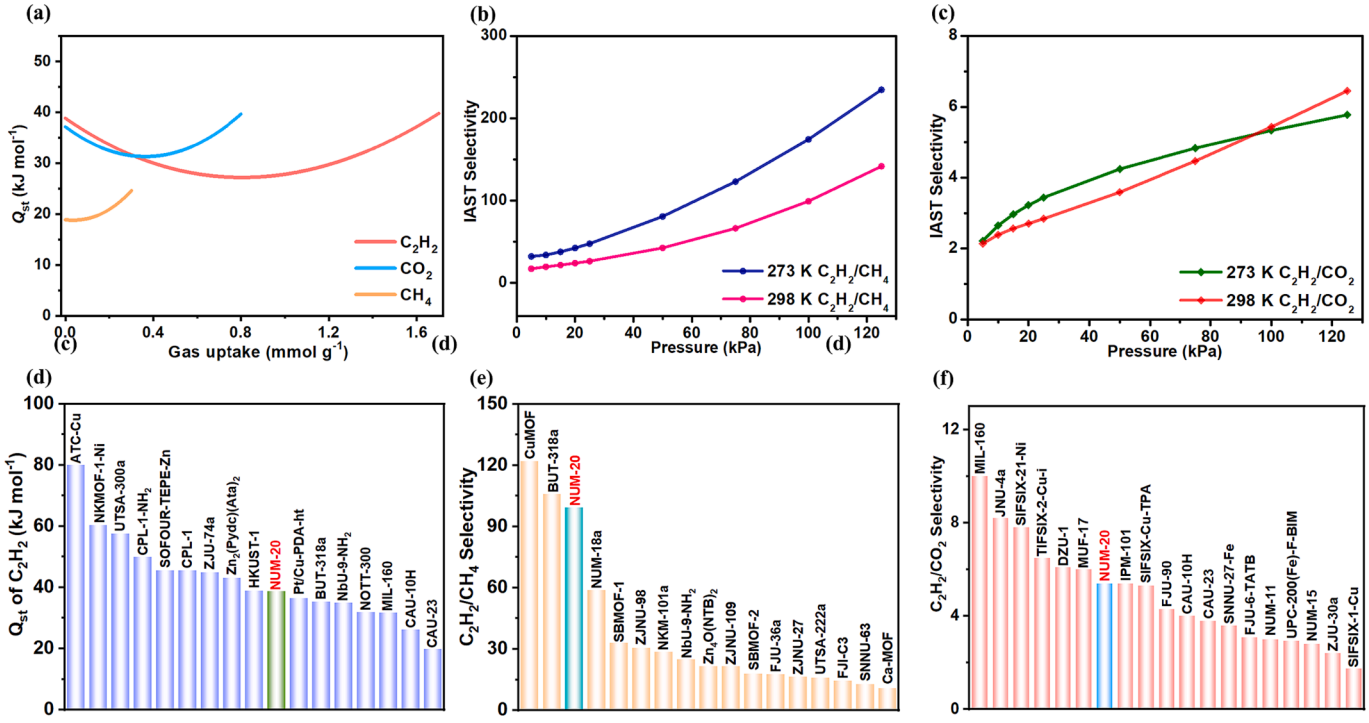

Fig. 4. (a) Isosteric heat of adsorption of C_2H_2, CO_2 and CH_4 in **NUM-20**. (b) Predicted mixture selectivity of **NUM-20** for equimolar C_2H_2/CH_4 mixture. (c) Predicted mixture selectivity of **NUM-20** for equimolar C_2H_2/CO_2 mixture. (d) Comparisons of low-coverage of Q_{st} value of C_2H_2 between **NUM-20** and other reported MOFs. (e) Comparisons of C_2H_2/CH_4 selectivity between **NUM-20** and other reported MOFs at ambient conditions. (f) Comparisons of C_2H_2/CO_2 selectivity between **NUM-20** and other reported MOFs at ambient conditions.

separation performance among Ca-based MOF adsorbents.

In order to verify the feasibility of purification of C_2H_2 from binary mixtures even multiple component mixtures containing CO_2 and CH_4 in the pressure swing adsorption process, the transient breakthrough simulations for the equimolar C_2H_2/CO_2, C_2H_2/CH_4, and $C_2H_2/CO_2/CH_4$ mixtures were carried out. As shown in Fig. 5a, b, it could be seen that clear separation could be achieved by **NUM-20**, whereby CO_2 and CH_4 breakthrough occurred first, followed by C_2H_2 after some time. The C_2H_2/CO_2 separation performance is higher or comparable than that of JXNU-12 [52], NUM-11 [53], while lower than that of JXNU-12 (F) [52], and MIL-160 [48], etc. It is remarkable that **NUM-20** could accomplish ternary mixture separation, which follows the breakthrough sequence with CH_4, CO_2, and C_2H_2 (Fig. 5c, d), lining with the adsorption isotherms tendency. In addition, the desorption simulations were performed to evaluate the obtained C_2H_2 purity. As shown in Figs. S5-S7, it affords a recovery C_2H_2 with high purity (>99%) whether binary mixtures or ternary mixture. In short, the results of all those breakthrough curves undoubtedly suggested that the **NUM-20** possesses the separation and purification capacity of C_2H_2 from mixtures containing one or more gaseous mixtures such as CH_4 and CO_2.

3.4. GCMC simulations

In order to better elaborate the mechanism for the preferential C_2H_2 adsorption and the different adsorption behavior for C_2H_2, CO_2 and CH_4 on **NUM-20**, the theoretical study using grand canonical Monte Carlo (GCMC) simulations was carried out to investigate the guest molecules including C_2H_2, CH_4, and CO_2 molecules adsorption performance of **NUM-20**. As shown in Fig. 6a, the preferential adsorption sites of the linear C_2H_2 molecule were distributed in the middle of multiple benzene rings and the C_2H_2 interacts with the skeleton via forming six C-H···π (3.308–3.972 Å) interactions. Unlike the C_2H_2 molecules, the preferential binding sites of CO_2 and CH_4 molecules are located near the Ca^{2+} ions and the corner near the aromatic rings. CO_2 molecule interacts with the skeleton by forming one O-Ca (2.807 Å) electrostatic interaction and four C-H···O (2.725–2.968 Å) interactions (Fig. 6b). And CH_4 molecule interacts with the skeleton by forming one C-Ca (3.934 Å) Coulombic interaction and two C-H···π (3.536–3.554 Å) interactions (Fig. 6c). In addition, density functional theory (DFT) calculations were performed to further qualitatively evaluate the preferential binding sites for the gas molecules within **NUM-20**, which agrees well with the GCMC simulations (Figs. S16-S18 and Table S2). Therefore, it could be seen from the above discussion that the stronger host–guest interaction drives the highest C_2H_2 binding affinity compared to CO_2 and CH_4 molecules and well capture and separation of C_2H_2 from C_2H_2-containing mixtures. These theoretical calculation results agreed well with the experimental performance.

4. Conclusions

In summary, we have synthesized a thermostable Ca-based metal–organic framework (**NUM-20**) and systematically studied the adsorption and separation performance of C_2H_2, CH_4, and CO_2 molecules and their mixtures. It is worth noting that **NUM-20** could selectively capture C_2H_2 from ternary mixtures as revealed by sorption isotherms, the heat of adsorption, IAST calculations and transient breakthrough simulations. The results of experiments and computations all suggest that **NUM-20** can be a candidate porous adsorbent for challenging gaseous mixtures separation. This work enriches the Ca-based MOF family and provides an efficient multifunctional porous adsorbent to address challenging multicomponent mixtures separation. It is expected that this kind of multifunctional adsorbent could be constructed by other biocompatible metals and may pave the route for their implementations in gas adsorption and separation.

CRediT authorship contribution statement

Shan-Qing Yang: Conceptualization, Methodology, Visualization,

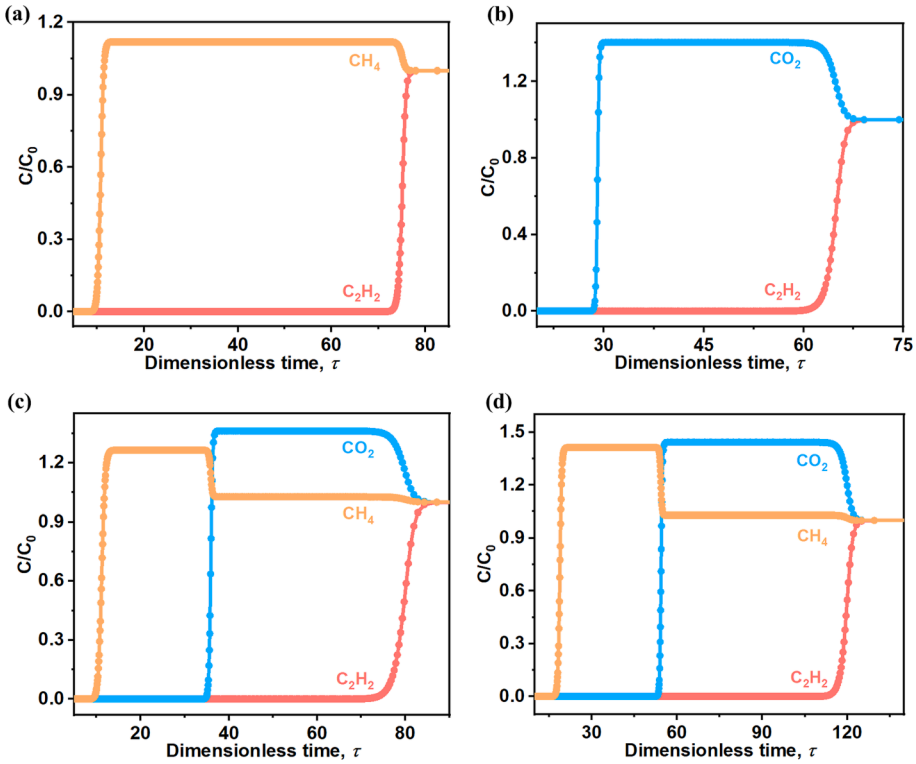

Fig. 5. Transient breakthrough simulations of equimolar mixtures including C_2H_2/CO_2 and C_2H_2/CH_4 binary mixtures, $C_2H_2/CH_4/CO_2$ ternary mixture, in an adsorber bed packed using **NUM-20**. Different operating conditions were (a) C_2H_2/CH_4 at 298 K, (b) C_2H_2/CO_2 at 298 K, (c) $C_2H_2/CO_2/CH_4$ at 298 K; (d) $C_2H_2/CO_2/CH_4$ at 273 K. The total bulk gas phase in the fixed bed is 100 kPa.

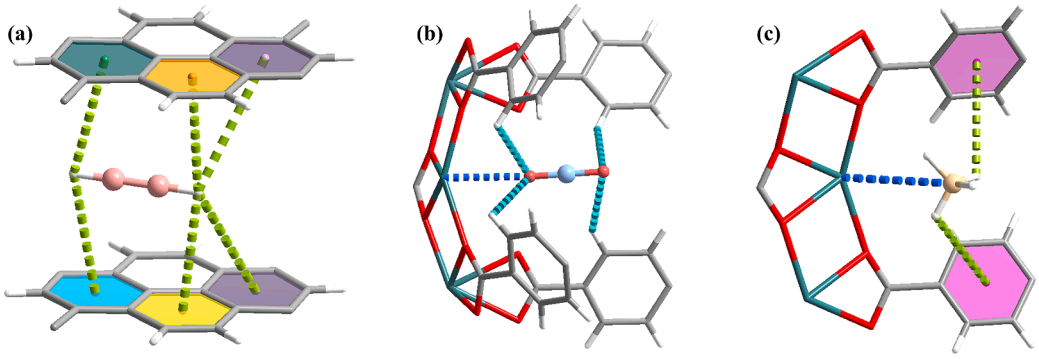

Fig. 6. Preferential adsorption sites calculated by GCMC simulations at 298 K and 1.0 bar for (a) C_2H_2, (b) CO_2, and (c) CH_4 in **NUM-20** (C, gray; O, red; Ca, green; and H, white.).

Investigation, Writing – original draft. **Rajamani Krishna:** Formal analysis, Methodology. **Lei Zhou:** Software, Formal analysis, Visualization. **Yi-Long Li:** Investigation. **Bo Xing:** Investigation. **Qiang Zhang:** Investigation. **Fei-Yang Zhang:** Investigation. **Tong-Liang Hu:** Supervision, Conceptualization, Project administration, Funding acquisition, Resources, Writing – review & editing.

Declaration of Competing Interest

The authors declare that they have no known competing financial interests or personal relationships that could have appeared to influence the work reported in this paper.

Data availability

No data was used for the research described in the article.

Acknowledgements

This work was financially supported by the National Natural Science Foundation of China (22275102). We would like to thank Professor Wei Li from Nankai University for his help in the simulation of the experiment.

Appendix A. Supplementary material

Supplementary data to this article can be found online at https://doi.org/10.1016/j.seppur.2023.125167.

References

[1] D.S. Sholl, R.P. Lively, Seven chemical separations to change the world, Nature 532 (2016) 435–437.
[2] S. Dutta, S. Mukherjee, O.T. Qazvini, A.K. Gupta, S. Sharma, D. Mahato, R. Babarao, S.K. Ghosh, Three-in-one C_2H_2-selectivity-guided adsorptive separation across an isoreticular family of cationic square-lattice MOFs, Angew. Chem. Int. Ed. 61 (2021) e202114132.
[3] A. Granada, S.B. Karra, S.M. Senkan, Conversion of methane into acetylene and ethylene by the chlorine-catalyzed oxidative-pyrolysis (CCOP) process. 1. Oxidative pyrolysis of chloromethane, Ind. Eng. Chem. Res. 26 (1987) 1901–1905.
[4] S. Mukherjee, D. Sensharma, K. Chen, M.J. Zaworotko, Crystal engineering of porous coordination networks to enable separation of C2 hydrocarbons, Chem. Commun. 56 (2020) 10419–10441.
[5] Y. Liu, J. Liu, H. Xiong, J. Chen, S. Chen, Z. Zeng, S. Deng, J. Wang, Negative electrostatic potentials in a Hofmann-type metal-organic framework for efficient acetylene separation, Nat. Commun. 13 (2022) 5515.
[6] J.-R. Li, R.J. Kuppler, H.-C. Zhou, Selective gas adsorption and separation in metal-organic frameworks, Chem. Soc. Rev. 38 (2009) 1477–1504.
[7] C.R. Reid, K.M. Thomas, Adsorption kinetics and size exclusion properties of probe molecules for the selective porosity in a carbon molecular sieve used for air separation, J. Phys. Chem. B 105 (2001) 10619–10629.
[8] S.-Q. Yang, T.-L. Hu, Reverse-selective metal-organic framework materials for the efficient separation and purification of light hydrocarbons, Coord. Chem. Rev. 468 (2022), 214628.
[9] Y.-L. Peng, T. Pham, P. Li, T. Wang, Y. Chen, K.-J. Chen, K.A. Forrest, B. Space, P. Cheng, M.J. Zaworotko, Z. Zhang, Robust ultramicroporous metal-organic frameworks with benchmark affinity for acetylene, Angew. Chem. Int. Ed. 57 (2018) 10971–10975.
[10] R.-B. Lin, L. Li, H. Wu, H. Arman, B. Li, R.-G. Lin, W. Zhou, B. Chen, Optimized separation of acetylene from carbon dioxide and ethylene in a microporous material, J. Am. Chem. Soc. 139 (2017) 8022–8028.
[11] S.-Q. Yang, R. Krishna, H. Chen, L. Li, L. Zhou, Y.-F. An, F.-Y. Zhang, Q. Zhang, Y.-H. Zhang, W. Li, T.-L. Hu, X.-H. Bu, Immobilization of the polar group into an ultramicroporous metal-organic framework enabling benchmark inverse selective CO_2/C_2H_2 separation with record C_2H_2 production, J. Am. Chem. Soc. 145 (2023) 13901–13911.
[12] M. Shivanna, K.-I. Otake, B.-Q. Song, L.M. van Wyk, Q.-Y. Yang, N. Kumar, W. K. Feldmann, T. Pham, S. Suepaul, B. Space, L.J. Barbour, S. Kitagawa, M. J. Zaworotko, Benchmark acetylene binding affinity and separation through induced fit in a flexible hybrid ultramicroporous material, Angew. Chem. Int. Ed. 60 (2021) 20383–20930.
[13] X. Zhu, T. Ke, J. Zhou, Y. Song, Q. Xu, Z. Zhang, Z. Bao, Y. Yang, Q. Ren, Q. Yang, Vertex strategy in layered 2D MOFs: Simultaneous improvement of thermodynamics and kinetics for record C_2H_2/CO_2 separation performance, J. Am. Chem. Soc. 145 (2023) 9254–9263.
[14] O.T. Qazvini, R. Babarao, S.G. Telfer, Selective capture of carbon dioxide from hydrocarbons using a metal-organic framework, Nat. Commun. 12 (2021) 197.
[15] D. Bai, X. Gao, M. He, Y. Wang, Y. He, Three isoreticular MOFs derived from nitrogen-functionalized diisophthalate ligands: exploring the positional effect of nitrogen functional sites on the structural stabilities and selective C_2H_2/CH_4 and CO_2/CH_4 adsorption properties, Inorg. Chem. Front. 5 (2018) 1423–1431.
[16] Y. Du, Y. Chen, Y. Wang, C. He, J. Yang, L. Li, J. Li, Optimized pore environment for efficient high selective C_2H_2/C_2H_4 and C_2H_2/CO_2 separation in a metal-organic framework, Sep. Purif. Technol. 256 (2021), 117749.
[17] Y. Zhang, X. Deng, X. Li, X. Liu, P. Zhang, L. Chen, Z. Yan, J. Wang, S. Deng, A stable metal-organic framework with oxygen site for efficiently trapping acetylene from acetylene-containing mixtures, Sep. Purif. Technol. 316 (2023), 123751.
[18] H. Furukawa, K.E. Cordova, M. O'Keeffe, O.M. Yaghi, The chemistry and applications of metal-organic frameworks, Science 341 (2013) 1230444.
[19] X. Zhang, Z. Chen, X. Liu, S.L. Hanna, X. Wang, R. Taheri-Ledari, A. Maleki, P. Li, O.K. Farha, A historical overview of the activation and porosity of metal-organic frameworks, Chem. Soc. Rev. 49 (2020) 7406–7427.
[20] D.K. Yoo, I. Ahmed, M. Sarker, H.J. Lee, A. Vinu, S.H. Jhung, Metal-organic frameworks containing uncoordinated nitrogen: Preparation, modification, and application in adsorption, Mater. Today 51 (2021) 566–585.
[21] D.-D. Zhou, X.-W. Zhang, Z.-W. Mo, Y.-Z. Xu, X.-Y. Tian, Y. Li, X.-M. Chen, J.-P. Zhang, Adsorptive separation of carbon dioxide: From conventional porous materials to metal-organic frameworks, EnergyChem 1 (2019), 100016.
[22] S. Xian, Y. Lin, H. Wang, J. Li, Calcium-based metal-organic frameworks and their potential applications, Small 17 (2021) 2005165.
[23] Z. Niu, X. Cui, T. Pham, G. Verma, P.C. Lan, C. Shan, H. Xing, K.A. Forrest, S. Suepaul, B. Space, A. Nafady, A.M. Al-Enizi, S. Ma, A MOF-based ultra-strong acetylene nano-trap for highly efficient C_2H_2/CO_2 separation, Angew. Chem. Int. Ed. 60 (2021) 5283–5288.
[24] Z. Zhang, S.B. Peh, Y. Wang, C. Kang, W. Fan, D. Zhao, Efficient trapping of trace acetylene from ethylene in an ultramicroporous metal-organic framework via synergistic effect of high-fensity open metal sites and electronegative sites, Angew. Chem. Int. Ed. 59 (2020) 18927–18932.
[25] L. Liu, Z. Yao, Y. Ye, Y. Yang, Q. Lin, Z. Zhang, M. O'Keeffe, S. Xiang, Integrating the pillared-layer strategy and pore-space partition method to construct multicomponent MOFs for C_2H_2/CO_2 separation, J. Am. Chem. Soc. 142 (2020) 9258–9266.
[26] H. Wang, N. Behera, S. Wang, Q. Dong, Z. Wang, B. Zheng, D. Wang, J. Duan, Optimized nanospace of coordination isomers with selenium sites for acetylene separation, Inorg. Chem. Front. 7 (2020) 3195–3203.

[27] Q. Li, N. Wu, J. Li, D. Wu, A highly connected trinuclear cluster based metal-organic framework for efficient separation of C_2H_2/C_2H_4 and C_2H_2/CO_2, Inorg. Chem. 59 (2020) 13005–13008.
[28] P.-D. Zhang, X.-Q. Wu, T. He, L.-H. Xie, Q. Chen, J.-R. Li, Selective adsorption and separation of C_2 hydrocarbons in a "flexible-robust" metal-organic framework based on a guest-dependent gate-opening effect, Chem. Commun. 56 (2020) 5520–5523.
[29] X. Jiang, T. Pham, J.-W. Cao, K.A. Forrest, H. Wang, J. Chen, Q.-Y. Zhang, K.-J. Chen, Molecular sieving of acetylene from ethylene in a rigid ultra-microporous metal organic framework, Chem Eur J 27 (2021) 9446–9453.
[30] X. Liu, P. Zhang, H. Xiong, Y. Zhang, K. Wu, J. Liu, R. Krishna, J. Chen, S. Chen, Z. Zeng, S. Deng, J. Wang, Engineering pore environments of sulfate-pillared metal-organic framework for efficient C_2H_2/CO_2 separation with record selectivity, Adv. Mater. 35 (2023) 2210415.
[31] G.-D. Wang, Y.-Z. Li, W.-F. Zhang, L. Hou, Y.-Y. Wang, Z. Zhu, Acetylene separation by a Ca-MOF containing accessible sites of open metal centers and organic groups, ACS Appl. Mater. Interfaces 13 (2021) 58862–58870.
[32] A.M. Plonka, X. Chen, H. Wang, R. Krishna, X. Dong, D. Banerjee, W.R. Woerner, Y. Han, J. Li, J.B. Parise, Light hydrocarbon adsorption mechanisms in two calcium-based microporous metal organic frameworks, Chem. Mater. 28 (2016) 1636–1646.
[33] N. Xu, J. Hu, L. Wang, D. Luo, W. Sun, Y. Hu, D. Wang, X. Cui, H. Xing, Y. Zhang, A TIFSIX pillared MOF with unprecedented zsd topology for efficient separation of acetylene from quaternary mixtures, Chem. Eng. J. 450 (2022), 138034.
[34] G.-D. Wang, H.-H. Wang, W.-J. Shi, L. Hou, Y.-Y. Wang, Z. Zhu, A highly stable MOF with F and N accessible sites for efficient capture and separation of acetylene from ternary mixtures, J. Mater. Chem. A 9 (2021) 24495–24502.
[35] G.M. Sheldrick, SHELXT - integrated space-group and crystal-structure determination, Acta Cryst. A 71 (2015) 3–8.
[36] G.M. Sheldrick, Crystal structure refinement with SHELXL, Acta Cryst. C 71 (2015) 3–8.
[37] D. McIntosh, The physical properties of liquid and solid acetylene, J. Phys. Chem. 11 (1907) 306–317.
[38] X. Rao, J. Cai, J. Yu, Y. He, C. Wu, W. Zhou, T. Yildirim, B. Chen, G. Qian, A microporous metal-organic framework with both open metal and Lewis basic pyridyl sites for high C_2H_2 and CH_4 storage at room temperature, Chem. Commun. 49 (2013) 6719–6721.
[39] S. Xiang, W. Zhou, J.M. Gallegos, Y. Liu, B. Chen, Exceptionally high acetylene uptake in a microporous metal-organic framework with open metal sites, J. Am. Chem. Soc. 131 (2009) 12415–12419.
[40] F. Moreau, I. da Silva, N.H. Al Smail, T.L. Easun, M. Savage, H.G.W. Godfrey, S. F. Parker, P. Manuel, S. Yang, M. Schröder, Unravelling exceptional acetylene and carbon dioxide adsorption within a tetra-amide functionalized metal-organic framework, Nat. Commun. 8 (2017) 14085.
[41] L. Zhang, K. Jiang, L. Yang, L. Li, E. Hu, L. Yang, K. Shao, H. Xing, Y. Cui, Y. Yang, B. Li, B. Chen, G. Qian, Benchmark C_2H_2/CO_2 separation in an ultra-microporous metal-organic framework via cpper(I)-alkynyl chemistry, Angew. Chem. Int. Ed. 60 (2021) 15995–16002.
[42] Y.-Y. Xue, X.-Y. Bai, J. Zhang, Y. Wang, S.-N. Li, Y.-C Jiang, M.-C. Hu, Q-G. Zhai, Precise pore space partitions combined with high-density hydrogen-bonding acceptors within metal-organic frameworks for highly efficient acetylene storage and separation, Angew. Chem. In. Ed. 60 (2021) 10122–10128.
[43] J. Pei, H.-M. Wen, X.-W. Gu, Q.-L. Qian, Y. Yang, Y. Cui, B. Li, B. Chen, G. Qian, Dense packing of acetylene in a stable and low-cost metal-organic framework for efficient C_2H_2/CO_2 separation, Angew. Chem. Int. Ed. 60 (2021) 25068–25074.
[44] H. Zeng, M. Xie, Y.-L. Huang, Y. Zhao, X.-J. Xie, J.-P. Bai, M.-Y. Wan, R. Krishna, W. Lu, D. Li, Induced fit of C_2H_2 in a flexible MOF through cooperative action of open metal sites, Angew. Chem. Int. Ed. 58 (2019) 8515–8519.
[45] Y. Ye, Z. Ma, R.-B. Lin, R. Krishna, W. Zhou, Q. Lin, Z. Zhang, S. Xiang, B. Chen, Pore space partition within a metal-organic framework for highly efficient C_2H_2/CO_2 separation, J. Am. Chem. Soc. 141 (2019) 4130–4136.
[46] W. Fan, S. Yuan, W. Wang, L. Feng, X. Liu, X. Zhang, X. Wang, Z. Kang, F. Dai, D. Yuan, D. Sun, H.-C. Zhou, Optimizing multivariate metal-organic frameworks for efficient C_2H_2/CO_2 separation, J. Am. Chem. Soc. 142 (2020) 8728–8737.
[47] O.T. Qazvini, R. Babarao, S.G. Telfer, Multipurpose metal-organic framework for the adsorption of acetylene: ethylene purification and carbon dioxide removal, Chem. Mater.. 31 (2019) 4919–4926.
[48] Y. Ye, S. Xian, H. Cui, K. Tan, L. Gong, B. Liang, T. Pham, H. Pandey, R. Krishna, P. C. Lan, K.A. Forrest, B. Space, T. Thonhauser, J. Li, S. Ma, Metal-organic framework based hydrogen-bonding nanotrap for efficient acetylene storage and separation, J. Am. Chem. Soc.. 144 (2022) 1681–1689.
[49] Y. Qiao, X. Chang, J. Zheng, M. Yi, Z. Chang, M.-H. Yu, X.-H. Bu, Self-interpenetrated water-stable microporous metal-organic framework toward storage and purification of light hydrocarbons, Inorg. Chem. 60 (2021) 2749–2755.
[50] F. Hu, Z. Di, M. Wu, J. Li, Building a robust 3D Ca-MOF by a new square Ca_4O SBU for purification of natural gas, Dalton Trans. 49 (2020) 8836–8840.
[51] Z.-C. Xu, J. Yu, P.-D. Zhang, Y.-L. Zhao, X.-Q. Wu, M. Zhao, X. Zhang, J.-R. Li, Efficient C_2H_2 separation from CO_2 and CH_4 within a microporous metal-organic framework of multiple functionalities, Ind. Eng. Chem. Res. 61 (2022) 16233–16239.
[52] X.-P. Fu, Y.-L. Wang, X.-F. Zhang, R. Krishna, C.-T. He, Q.-Y. Liu, B. Chen, Collaborative pore partition and pore surface fluorination within a metal–organic framework for high-performance C_2H_2/CO_2 separation, Chem. Eng. J. 432 (2022), 134433.
[53] S.-Q. Yang, L. Zhou, Y. He, R. Krishna, Q. Zhang, Y.-F. An, B. Xing, Y.-H. Zhang, T.-L. Hu, Two-dimensional metal-organic framework with ultrahigh water stability for separation of acetylene from carbon dioxide and ethylene, ACS Appl. Mater. Interfaces 14 (2022) 33429–33437.

Supporting Information

A thermostable calcium-based metal-organic framework for efficient capture and separation of acetylene from ternary mixture

Shan-Qing Yang,[a] Rajamani Krishna,[b] Lei Zhou,[a] Yi-Long Li,[a] Bo Xing,[a] Qiang Zhang,[a] Fei-Yang Zhang,[a] Tong-Liang Hu*[a]

[a] School of Materials Science and Engineering, National Institute for Advanced Materials, Nankai University, Tianjin 300350, China. Email: tlhu@nankai.edu.cn (T.-L. Hu)

[b] Van 't Hoff Institute for Molecular Sciences, University of Amsterdam, Science Park 904, 1098 XH Amsterdam, The Netherlands.

Experimental Section

Transient breakthrough simulations

Transient breakthrough simulations were carried out using the methodology described in earlier publications [1-5]. In these simulations, intra-crystalline diffusion influences are ignored.

The simulations were performed in a fixed bed with the following parameters: adsorber length, L = 0.3 m; cross-sectional area, A = 1 m^2; interstitial gas velocity in the bed, v = 0.1 m s^{-1}; voidage of the packed bed, ε = 0.4; the superficial gas velocity at the inlet to the bed, u = 0.04 m s^{-1}. The volumetric flow rate of the gas mixture at the inlet Q_0 = 40 L s^{-1}. The volume of MOF used in the simulations is $V_{ads} = LA(1-\varepsilon)$ = 0.18 m^3. Also, note that since the superficial gas velocity is specified, the specification of the cross-sectional area of the tube, A, is not relevant in the simulation results presented; essentially, we set A = 1 m^2. The total volume of the bed is $V_{bed} = LA$. It is important to note that the volume of adsorbent, V_{ads}, includes the pore volume of the adsorbent material. If ρ is the framework density, the mass of the adsorbent in the bed is $m_{ads} = (1-\varepsilon)\times(L \text{ m})\times(A \text{ m}^2)\times(\rho \text{ kg m}^{-3})$ kg.

For presentation of the results of the breakthrough simulations, the dimensionless concentrations at the exit, c_i/c_{i0} are plotted as a function of the dimensionless parameter $\tau = \dfrac{tu}{L\varepsilon}$, defined by dividing the actual time, t, by the characteristic time, $\dfrac{L\varepsilon}{u}$.

DFT Calculation

All density functional theory (DFT) calculations were performed using the Vienna Ab initio Simulation Package (VASP) [6,7] at the level of generalized gradient approximation (GGA) using Perdew-Burke-Ernzerhof (PBE) exchange-correlation functional [8]. Projector-augmented wave (PAW) potentials were used to describe the effective cores [9,10]. The valence electrons of all atoms were expanded in a plane wave basis set with a cutoff energy of 400 eV. The atomic structures were relaxed using either the conjugate gradient algorithm or the quasi-Newton scheme as implemented in the VASP code until the forces were less than 0.05 eV/Å for all unconstrained atoms, and the energy convergence criteria for all self-consistent field calculations were set as 10^{-4} eV. The van der Waals dispersion interaction between MOF and gas molecules was also considered by introducing the DFT-D3 method of Grimme [11]. The lattice parameters of **NUM-20** were a = 13.319 Å, b = 15.028 Å, c = 16.573 Å, so the sampling of Brillouin zone was only with Γ point [12].

The adsorption energy was defined as

$$E_{ads} = E(\text{MOF/M}) - E(\text{MOF}) - E(\text{M})$$

where the E(MOF/M), E(MOF) and E(M) represent the total energies of MOF with the adsorbate, the optimized MOF structure and the isolated gas molecules, respectively.

Fitting of Pure Component Isotherms

The isotherm data for C_2H_2, CH_4 and CO_2 in **NUM-20**, measured at 273 and 298 K were fitted with the Dual-site Langmuir-Freundlich model.

$$q = q_{A,sat} \frac{b_A p^{c_A}}{1 + b_A p^{c_A}} + q_{B,sat} \frac{b_B p^{c_B}}{1 + b_B p^{c_B}}$$

Calculation for C_2H_2/CH_4 and C_2H_2/CO_2 Adsorption Selectivities

The ideal adsorbed solution theory (IAST) was used to estimate the composition of the adsorbed phase from the data of single component isotherms and predict the selectivities of binary mixtures C_2H_2/CH_4 and C_2H_2/CO_2. IAST calculations of C_2H_2/CH_4 (50/50, v/v,) and C_2H_2/CO_2 (50/50, v/v) mixtures adsorption at 273 and 298 K, respectively were performed by

$$S_{ads} = \frac{q_1/q_2}{p_1/p_2}.$$

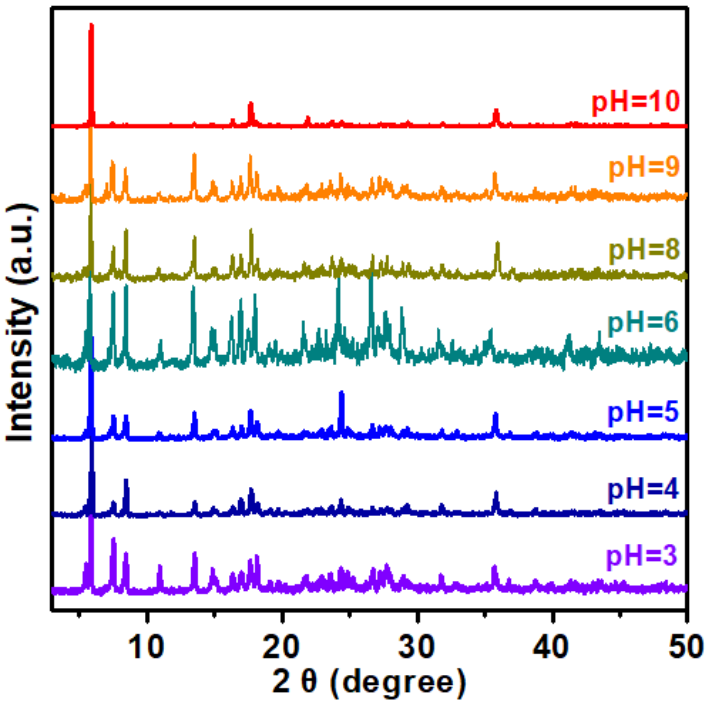

Figure S1. PXRD patterns for **NUM-20** in different pH value aqueous solutions for 12 h.

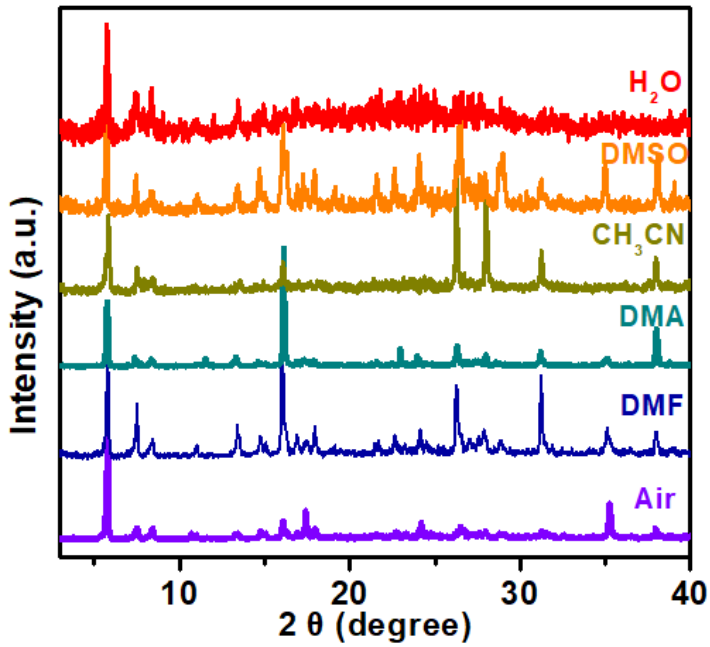

Figure S2. PXRD patterns for **NUM-20** in some organic solvents and air atmosphere for 24 h.

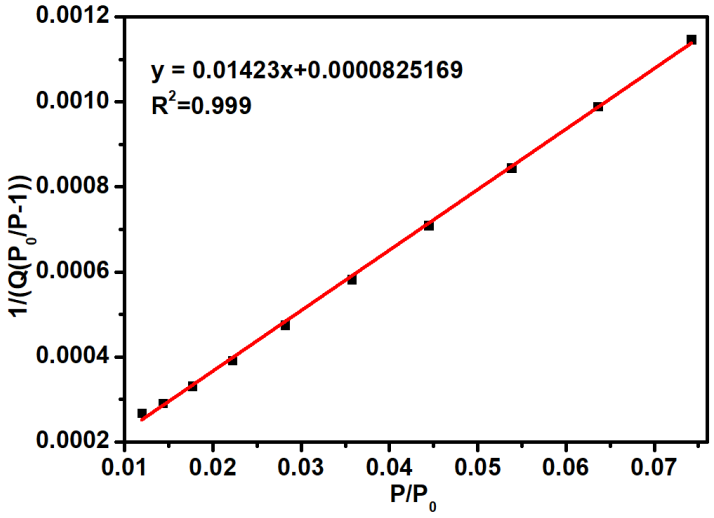

Figure S3. Calculation of BET surface area for **NUM-20** based on CO_2 adsorption isotherm at 195 K.

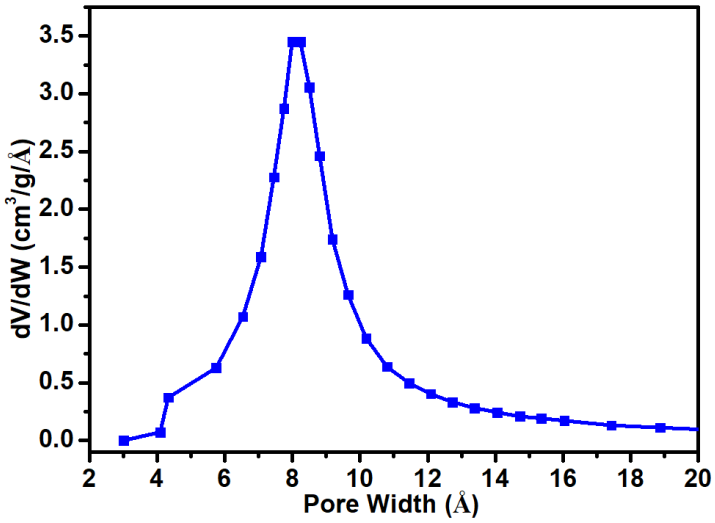

Figure S4. Pore size distribution of **NUM-20**.

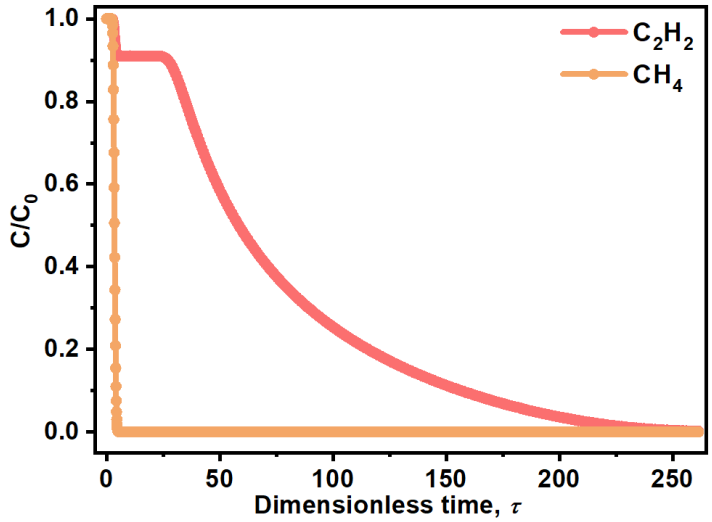

Figure S5. The desorption simulations of equimolar C_2H_2/CH_4 mixture.

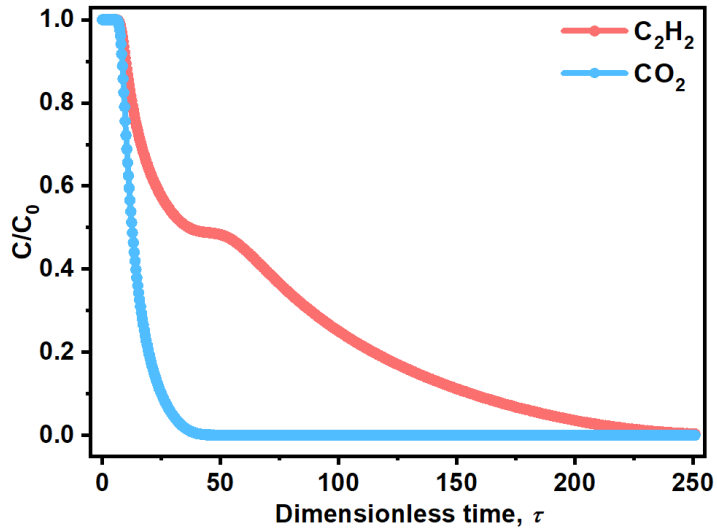

Figure S6. The desorption simulations of equimolar C_2H_2/CO_2 mixture.

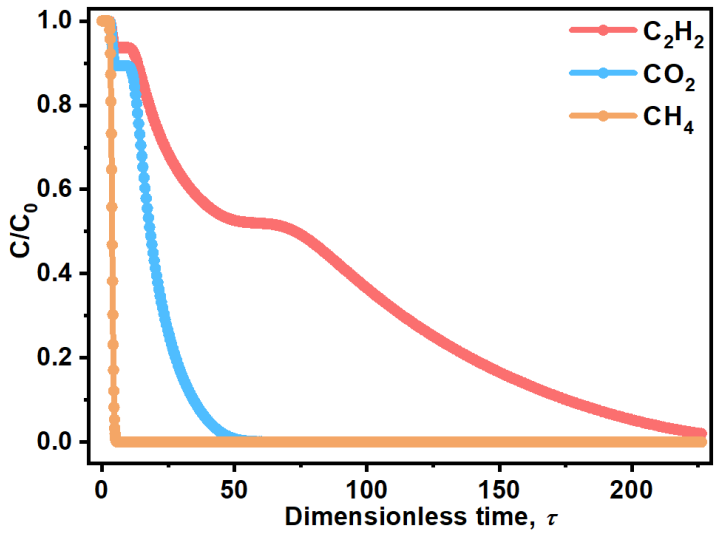

Figure S7. The desorption simulations of equimolar $C_2H_2/CH_4/CO_2$ mixture.

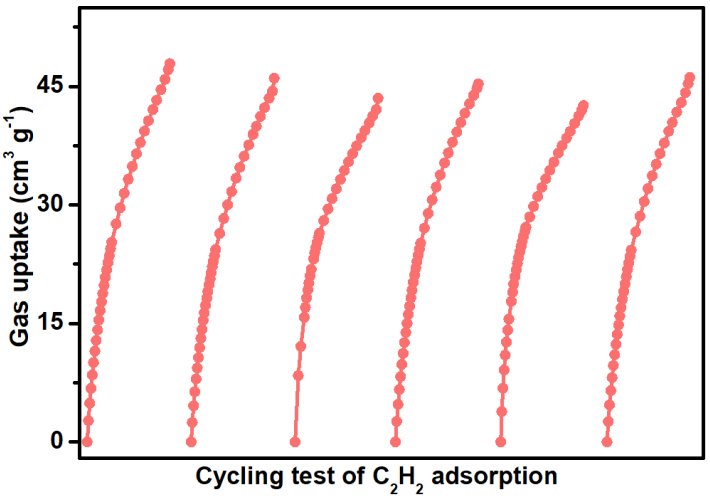

Figure S8. Cycling test of C_2H_2 adsorption measurements at 298 K.

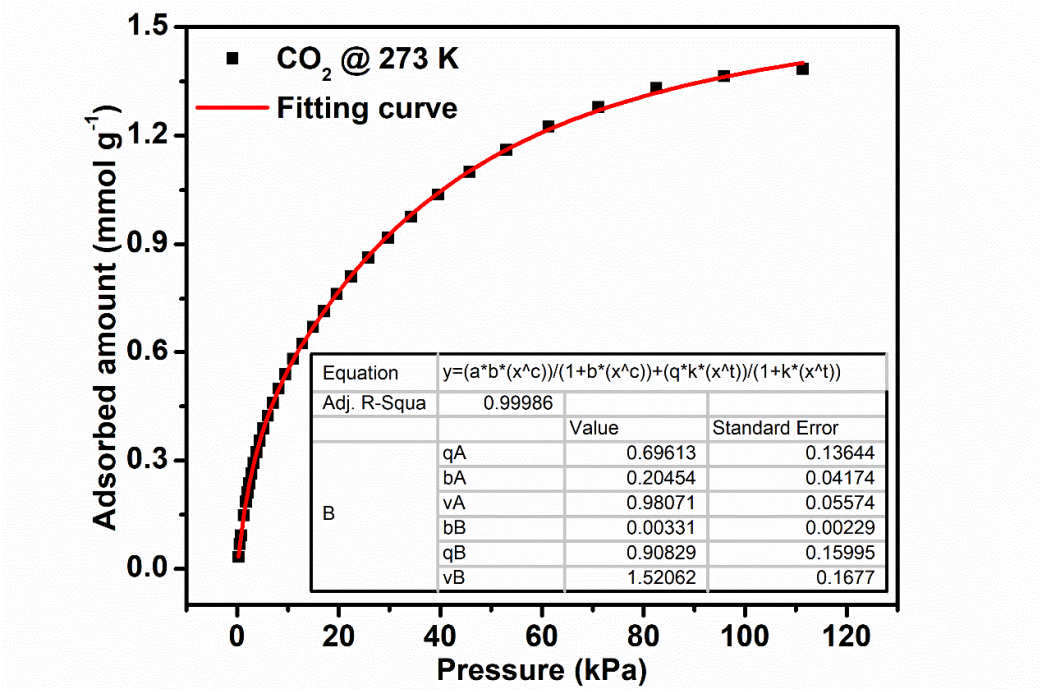

Figure S9. Dual-site Langmuir-Freundlich model for CO_2 adsorption isotherm on **NUM-20** at 273 K.

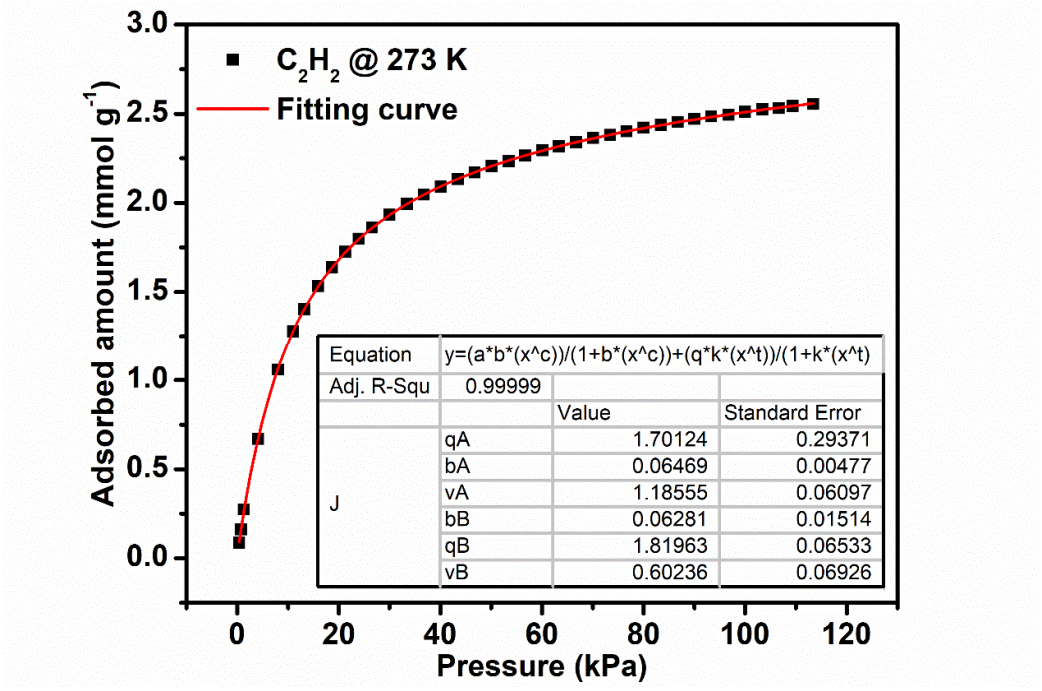

Figure S10. Dual-site Langmuir-Freundlich model for C_2H_2 adsorption isotherm on **NUM-20** at 273 K.

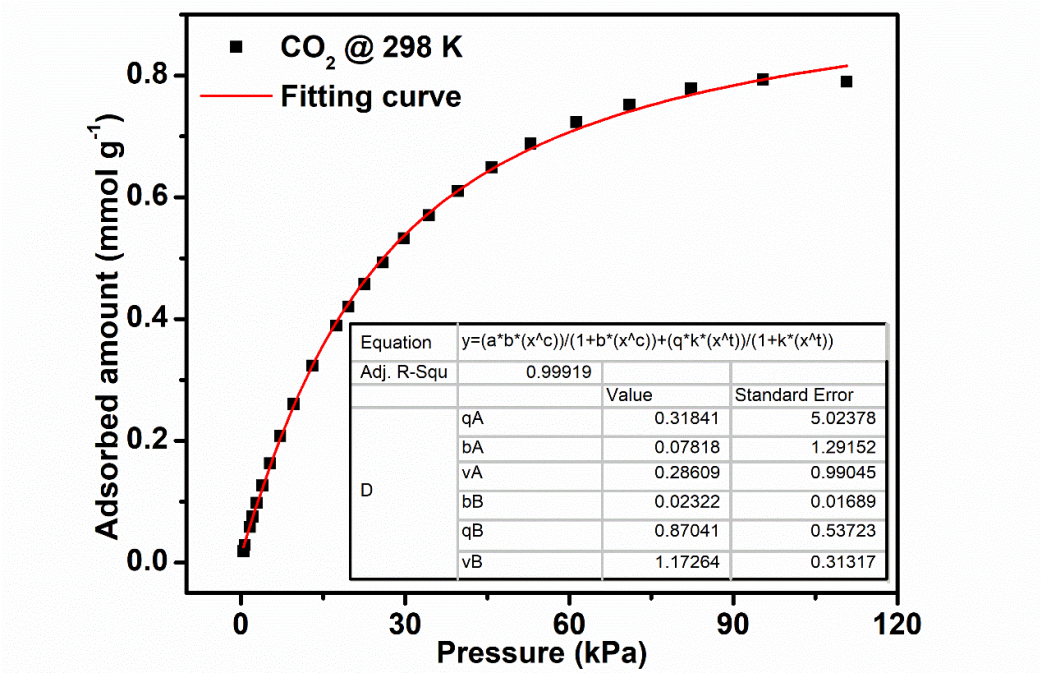

Figure S11. Dual-site Langmuir-Freundlich model for CO_2 adsorption isotherm on **NUM-20** at 298 K.

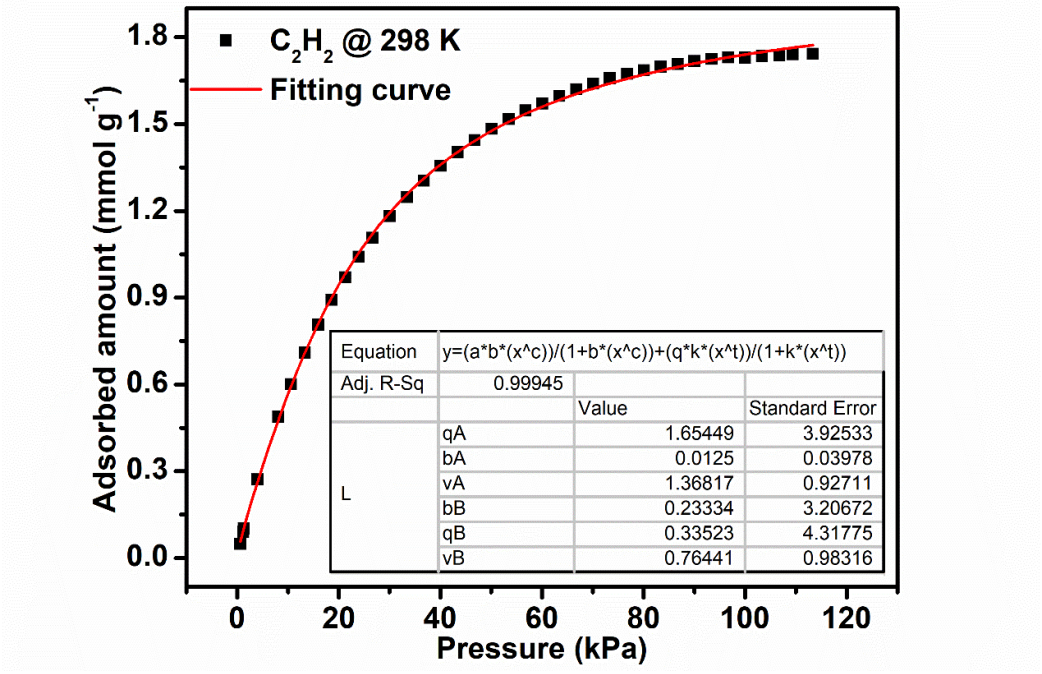

Figure S12. Dual-site Langmuir-Freundlich model for C_2H_2 adsorption isotherm on **NUM-20** at 298 K.

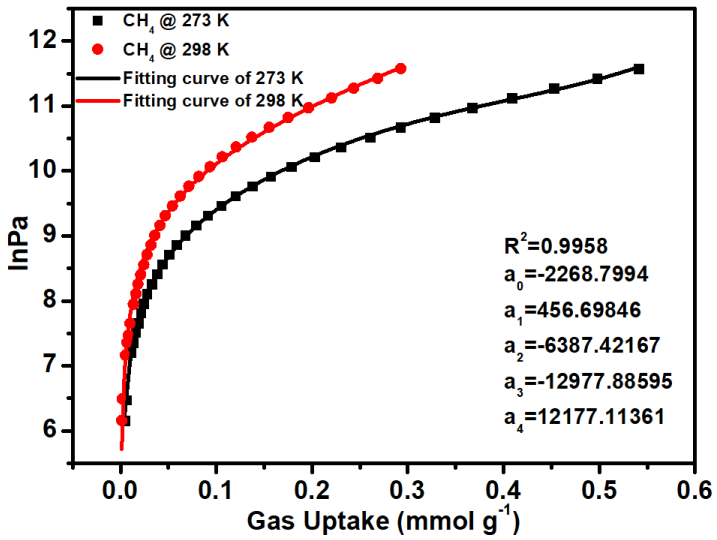

Figure S13. The details of virial equation (solid lines) fitting to the experimental CH_4 adsorption data (symbols) for **NUM-20**.

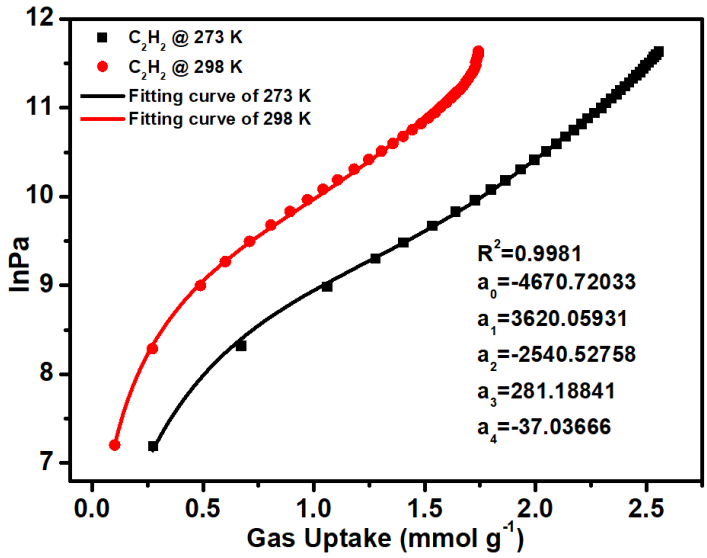

Figure S14. The details of virial equation (solid lines) fitting to the experimental C_2H_2 adsorption data (symbols) for **NUM-20**.

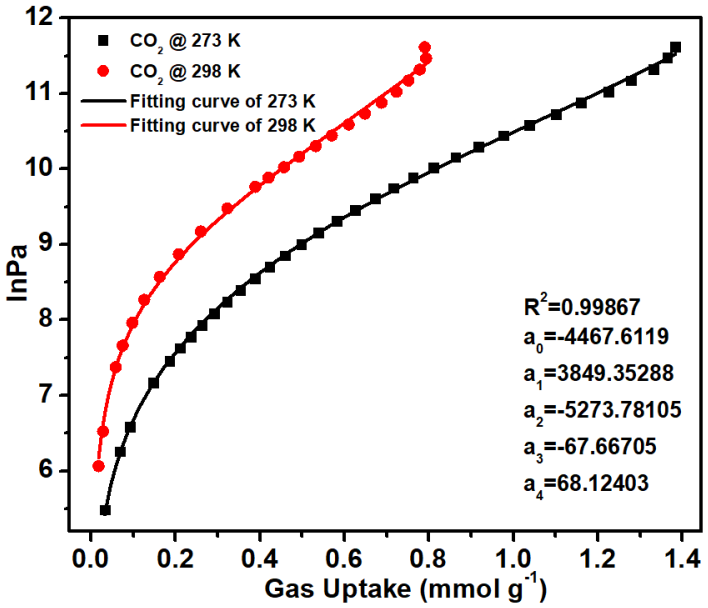

Figure S15. The details of virial equation (solid lines) fitting to the experimental CO_2 adsorption data (symbols) for **NUM-20**.

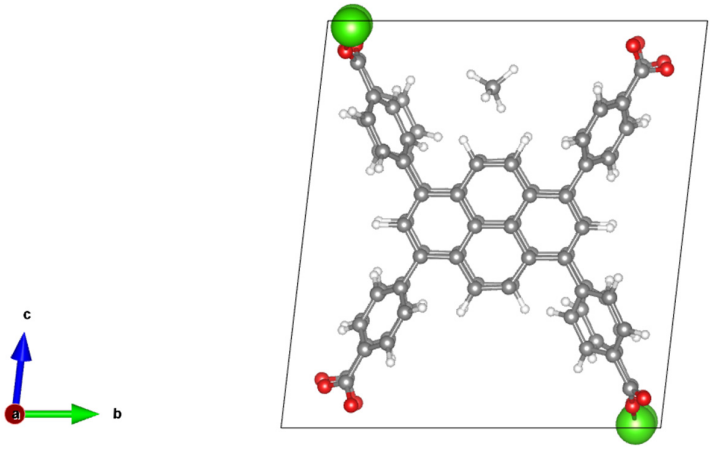

Figure S16. The DFT calculated adsorption energy of gas molecule at the site I of the **NUM-20**.

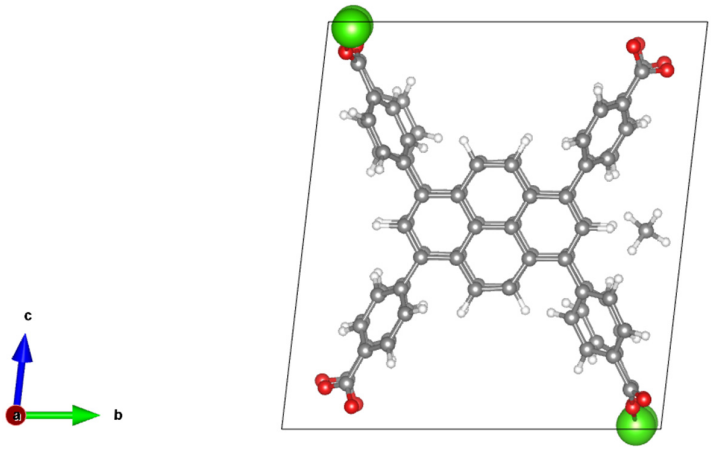

Figure S17. The DFT calculated adsorption energy of gas molecule at the site II of the **NUM-20**.

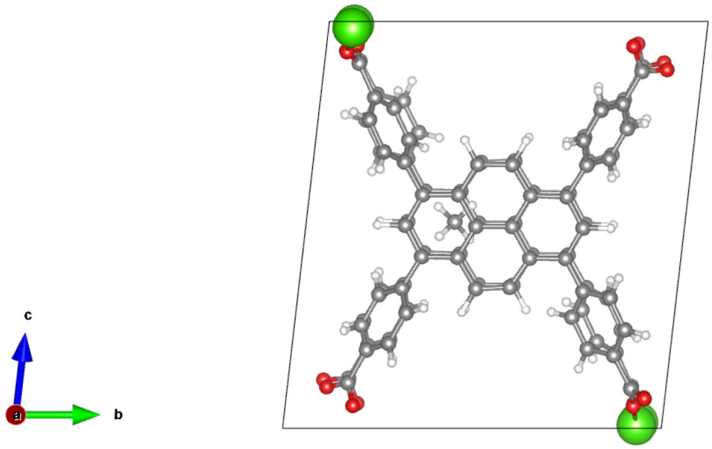

Figure S18. The DFT calculated adsorption energy of gas molecule at the site III of the **NUM-20**.

Table S1. The summary of energy of gas molecule and framework.

	C_2H_2	CO_2	CH_4	NUM-20
Energy/eV	-22.95	-23.00	-24.03	-1098.53

Table S2. The summary of energy of binding site.

	C_2H_2			CO_2			CH_4		
Site	SI	SII	SIII	SI	SII	SIII	SI	SII	SIII
Energy/ eV	-1121.65	-1121.73	-1121.76	-1121.74	-1122.03	-1121.87	-1122.70	-1122.85	-1122.81
E_{ads}/eV	-0.17	-0.25	-0.28	-0.21	-0.50	-0.34	-0.14	-0.29	-0.25

Table S3. Crystallographic parameters and refinement details of **NUM-20** ([Ca_2(TBAPy)(H_2O)$_4$·Solvents])

	NUM-20
Formula	$C_{44}H_{30}Ca_2O_{12}$
*M*r (g mol^{-1})	830.84
Crystal system	triclinic
Space group	*P*-1
a (Å)	13.3190(3)
b (Å)	15.0280(3)
c (Å)	16.5732(4)
α (°)	83.54(2)
β (°)	78.30(2)
γ (°)	89.94(2)
V (Å^3)	3226.87(1)
Z	2
D_c (g cm^{-3})	0.855
F (000)	860.0
μ (mm^{-1})	1.873
GOF on F^2	1.082
R_1, wR_2 [$I>2\sigma(I)$][a]	0.1021, 0.2908
R_1, wR_2 [all data][b]	0.1070, 0.2950

[a] $R_1 = \sum ||F_o| - |F_c|| / \sum |F_o|$. [b] $wR_2 = \{\sum[w(F_o^2 - F_c^2)^2] / \sum w(F_o^2)^2\}^{1/2}$

Table S4. A comparison of the gas adsorption and separation performance with reported adsorbents at ambient conditions.

	C_2H_2 uptake ($cm^3\ g^{-1}$)	C_2H_2/CO_2 selectivity	C_2H_2/CH_4 selectivity	Reference
$Zn(bdc)_{0.5}(mtrz)$	41.9	3.1	13.2	[13]
Cu-CPAH	131.8	3.6	20.3	[14]
$Zn_2(Pydc)(Ata)_2$	47.2	3.9	15.9	[15]
ZJU-13	115	4	20	[16]
$Zn(cpna)_3(tmbpy)$	71.25	3.9	22.4	[17]
NbU-11	77.3	2.5	175.8	[18]
Ni(dpip)	83.6	2	16.6	[19]
BUT-318a	51.46	5.5	105.8	[20]
BSF-1	52.5	3.3	46.9	[21]
SNNU-63	91.1	3.3	12.9	[22]
FJU-36a	52.2	2.8	17.7	[23]
NUM-20	39.03	5.4	99.3	This work

References

[1] R. Krishna, The Maxwell-Stefan description of mixture diffusion in nanoporous crystalline materials, Micropor. Mesopor. Mater. 185 (2014) 30-50.

[2] R. Krishna, Methodologies for evaluation of metal-organic frameworks in separation applications, RSC Adv. 5 (2015) 52269-52295.

[3] R. Krishna, Screening metal-organic frameworks for mixture separations in fixed-bed adsorbers using a combined selectivity/capacity metric, RSC Adv. 7 (2017) 35724-35737.

[4] R. Krishna, Methodologies for screening and selection of crystalline microporous materials in mixture separations, Sep. Purif. Technol. 194 (2018) 281-300.

[5] R. Krishna, Metrics for evaluation and screening of metal-organic frameworks for applications in mixture separations, ACS Omega 5 (2020) 16987-17004.

[6] G. Kresse, J. Furthmüller, Efficient iterative schemes for ab initio total-energy calculations using a plane-wave basis set, Phys. Rev. B: Condens. Matter Mater. Phys. 54 (1996) 11169.

[7] G. Kresse, J. Furthmüller, Efficiency of ab-initio total energy calculations for metals and semiconductors using a plane-wave basis set, Comput. Mater. Sci. 6 (1996) 15-50.

[8] J.P. Perdew, K. Burke, M. Ernzerhof, Generalized gradient approximation made simple, Phys. Rev. Lett. 77 (1996) 3865.

[9] G. Kresse, D. Joubert, From ultrasoft pseudopotentials to the projector augmented-wave method, Phys. Rev. B: Condens. Matter Mater. Phys. 59 (1999) 1758.

[10] P. E. Blöchl, Projector augmented-wave method, Phys. Rev. B: Condens. Matter Mater. Phys. 50 (1994) 17953.

[11] S. Grimme, J. Antony, S. Ehrlich, H. Krieg, A consistent and accurate ab initio parametrization of density functional dispersion correction (DFT-D) for the 94 elements H-Pu, J. Chem. Phys. 132 (2010) 154104.

[12] H. J. Monkhorst, J.D. Pack, Special points for Brillouin-zone integrations, Phys. Rev. B: Condens. Matter Mater. Phys. 13 (1976) 5188.

[13] Z.-H. Wang, R.-H. Su, G.-D. Wang, W.-J. Shi, L. Hou, Methyl-functionalized Zn-MOF for selective adsorption and separation of acetylene, J. Environ. Chem. Eng. 11 (2023) 110488.

[14] L. Meng, L. Yang, C. Chen, X. Dong, S. Ren, G. Li, Y. Han, Z, Shi, S. Feng, Selective acetylene adsorption within an imino-functionalized nanocage-based metal-organic framework, ACS Appl. Mater. Interfaces 12 (2020) 5999-6006.

[15] N. Xu, Y. Jiang, W. Sun, J. Li, L. Wang, Y. Jin, Y. Zhang, D. Wang, S. Duttwyler, Gram-scale synthesis of an ultrastable microporous metal-organic framework for efficient adsorptive separation of C_2H_2/CO_2 and C_2H_2/CH_4, Molecules 26 (2021) 5121.

[16] X. Duan, T. Xia, Z. Ji, Y. Cui, Y. Yang, G. Qian, A new microporous metal-organic framework for highly selective C_2H_2/CH_4 and C_2H_2/CO_2 separation at room temperature, Chin. J. Chem. 35 (2017) 1289-1293.

[17] P. Yan, J. Yang, X. Hao, Z. Chen, G. Shen, Y. Zhao, D. Ma, J. Zhu, A microporous zinc–organic framework with Lewis basic pyridyl sites for highly selective C_2H_2/CH_4 and C_2H_2/CO_2 gas separation, CrystEngComm 22 (2020)275-282.

[18] N. Wu, Q. Li, J. Li, D. Wu, Y. Li, 4-Connected cobalt-based 3D framework with a high affinity for acetylene, Inorg. Chem. 59 (2020) 9461-9464.

[19] Y.-Z. Li, G.-D. Wang, L.-N. Ma, L. Hou, Y.-Y. Wang, Z. Zhu, Multiple functions of gas separation and vapor adsorption in a new MOF with open tubular channels, ACS Appl. Mater. Interfaces 13 (2021) 4102-4109.

[20] Z.-C. Xu, J. Yu, P.-D. Zhang, Y.-L. Zhao, X.-Q. Wu, M. Zhao, X. Zhang, J.-R. Li, Efficient C_2H_2 separation from CO_2 and CH_4 within a microporous metal-organic framework of multiple functionalities, Ind. Eng. Chem. Res. 61 (2022) 16233-16239.

[21] Y. Zhang, L. Yang, L. Wang, S. Duttwyler H. Xing, A microporous metal-organic framework supramolecularly assembled from a Cu(II) dodecaborate cluster complex for selective gas separation. Angew. Chem. Int. Ed. 58 (2019) 8145-8150.

[22] Y.-T. Li, J.-W. Zhang, H.-J. Lv, M.-C. Hu, S.-N. Li, Y.-C. Jiang, Q.-G. Zhai, Tailoring the pore environment of a robust Ga-MOF by deformed $[Ga_3O(COO)_6]$ cluster for boosting C_2H_2 uptake and

separation, Inorg. Chem. 59 (2020) 10368-10373.

[23] L. Liu, Z. Yao, Y. Ye, L. Chen, Q. Lin, Y. Yang, Z. Zhang, S. Xiang, Robustness, selective gas separation, and nitrobenzene sensing on two isomers of cadmium metal-organic frameworks containing Various metal-O-metal chains, Inorg. Chem. 57 (2018) 12961-12968.